Key Engineering Materials
ISSN: 1662-9795, Vol. 1048, pp 133-150
doi:10.4028/p-0NIiBN

Submitted: 2026-01-19
Revised: 2026-02-16
Accepted: 2026-02-25
Online: 2026-04-14

Comparative Characterization through Torsion Tests of Primary and Secondary Aluminum Alloys for the Extrusion Process

Nicola Lai[1,a *], Sara Di Donato[1,b], Lorenzo Donati[1,c], Riccardo Pelaccia[2,d], Barbara Reggiani[2,e] and Marco Negozio[3,f]

[1]University of Bologna - DIN Department of Industrial Engineering, Viale Risorgimento 2, 40136, Bologna, Italy

[2]University of Modena and Reggio Emilia - DISMI Department of Sciences and Methods for Engineering, Via Amendola 2, 42122, Reggio Emilia, Italy

[3]University of Parma - DISTI Department for Industrial Systems and Technologies, Parco Area delle Scienze, 181/A, 43124 Parma, Italy

[a]nicola.lai5@unibo.it, [b]sara.didonato2@unibo.it, [c]l.donati@unibo.it, [d]riccardo.pelaccia@unimore.it, [e]barbara.reggiani@unimore.it, [f]marco.negozio@unipr.it

Keywords: Aluminum alloys, torsion tests, extrusion, secondary alloys, flow stress modeling.

Abstract. In the transition to a circular economy in the automotive sector, it is essential to integrate recycled (or secondary) aluminum alloys into extrusion processes, while ensuring that their performance is as close as possible to that of primary alloys. Within the Horizon Europe ZEvRA project, this study aims to analyze and investigate the hot deformation behavior of four aluminum alloys: two AA6082 alloys (primary and recycled) to directly assess their suitability for alternative use from a sustainability perspective, and two widely used automotive alloys, recycled AA6061 and primary AA7108, to provide reference data for industrial applications. Hot torsion tests were conducted under temperature and strain rate conditions representative of industrial extrusion processes. Four different temperatures (400, 450, 500, and 550 °C) and four different strain rates (0.01, 0.1, 1, and 10 s^{-1}) were investigated, allowing the achievement of significantly higher strain levels compared to conventional standard tensile and compression tests. Subsequently, the flow stress curves obtained from the torsion tests were analyzed to evaluate the influence of temperature and strain rate on the plastic deformation behavior of the material and on the associated dynamic softening mechanisms. The results demonstrate a comparable deformation behavior between primary and secondary alloys, confirming the feasibility and full compatibility of recycled alloys for high-performance industrial extrusion applications. Furthermore, experimental results provide a solid basis for the development of robust constitutive models to support FEM simulations aimed at optimizing metal forming processes within a circular manufacturing framework.

Introduction

The increase in demand for electric vehicles and the goals for carbon-neutral production have further accelerated the adoption of circular economy practices in the automotive industry. Supporting these strategies is the use of aluminum alloys, which are valued for their recyclability and lightweight properties. In particular, comparing primary and recycled AA6082 enables a direct assessment of the potential for sustainable alternative use in industrial extrusion processes, as recycled aluminum can reduce energy consumption by up to 95% and CO_2 emissions by more than 90 % [1–3]. However, many current extrusion processes still rely on primary alloys due to the strict compositional tolerances required for these materials. Integrating end-of-life scrap into extrusion processes requires not only the design of aluminum alloys with broader compositional tolerances, but also more advanced process control to ensure the required mechanical properties and microstructural stability [4–7]. In addition to the aforementioned alloys, which are essential for a comparison from an industrial sustainability perspective, this work also includes the hot characterization of recycled AA6061 and primary AA7108. These alloys are widely used in the automotive sector, and their analysis provides valuable reference data for key industrial materials, tested under the same conditions as AA6082.

Microstructural evolution plays a fundamental role during hot extrusion, strongly influencing material strength, crashworthiness, and corrosion resistance. The fibrous grain structure typical of extruded profiles enhances mechanical performance, whereas uncontrolled recrystallization can compromise component reliability. Restoration mechanisms such as dynamic recovery (DRV) and dynamic recrystallization (DRX), including continuous (CDRX) and geometric (GDRX) variants, are governed by temperature, strain rate, and alloy chemistry [8–14]. The prediction of these phenomena remains challenging due to their nonlinear dependence on process parameters and the interplay between stored energy and dispersoid drag [10–13].

At the same time, in recent years, FEM simulations have become increasingly important for optimizing extrusion processes, enabling improvements in die design, flow balancing, and thermal process analysis, while also reducing experimental costs [4–7]. Accurate prediction of microstructural evolution and flow stress behavior requires reliable and precise material cards. The Johnson-Cook model fails to capture complex coupled effects such as progressive dynamic recrystallization and stage-wise softening, whereas models based on Arrhenius equations and physical parameters provide greater accuracy thanks to Zener–Hollomon scaling and deformation-dependent parameters [15–20]. Reliable calibration of these models requires experimental data covering a wide range of strain values under specific thermal and kinematic conditions. This can be achieved through hot torsion testing, which overcomes the limitations of conventional tests such as tension and compression [9,14].

In the context of sustainable production, the assessment of the hot deformation behavior of aluminum alloys plays a strategic role in understanding their processability. This study provides a general evaluation of AA6061 Recycled and AA7108 alloys, along with a direct comparison between AA6082 Primary and AA6082 Recycled. The analysis focuses on the post-peak softening region of the flow stress curve, systematically examining the initial and final slopes of the curve, which are regarded as sensitive indicators of microstructural evolution during hot deformation.

This work aims to experimentally characterize the hot deformation behavior of the four previously mentioned aluminum alloys. To this end, hot torsion tests were performed at four different temperatures (400, 450, 500, and 550 °C) and four strain rates (0.01, 0.1, 1, and 10 s^{-1}). The flow stress curves were analyzed in the $\ln(\sigma)$–$\ln(\varepsilon)$ domain to better investigate the softening behavior after the peak stress. As previously mentioned, this region was divided into two main zones: the one immediately following the peak and the one preceding specimen fracture. This analysis makes it possible to assess the influence of temperature and strain rate on the mechanical behavior of each alloy. The results provide insights into the softening mechanisms and highlight the importance of characterization through hot torsion testing as a foundation for improving material models for FEM simulations and process design within a circular economy framework.

Materials and Method

Torsion Test. Hot torsion tests were carried out using solid cylindrical aluminum specimens with a central gauge section 10 mm in both length and diameter (Fig. 1). This geometry allows easier temperature control in the gauge section and enables the application of higher torque levels and larger strains before fracture compared to hollow tubular specimens. The specimen geometry includes an axial hole with a diameter of 3 mm and a length of 52.5 mm, which allows a thermocouple to be positioned close to the gauge section, enabling continuous temperature monitoring throughout the test. Before the application of torque, the specimen was heated using a solenoidal copper induction coil with a heating rate of 1 °C/s up to the target test temperature, followed by a 5-minute holding time. This procedure ensures a more uniform temperature distribution along the gauge section (Fig. 2). The temperature measured by the thermocouple was used as input for a PID controller, which maintained the temperature within ±1 °C of the target value throughout the entire duration of the test.

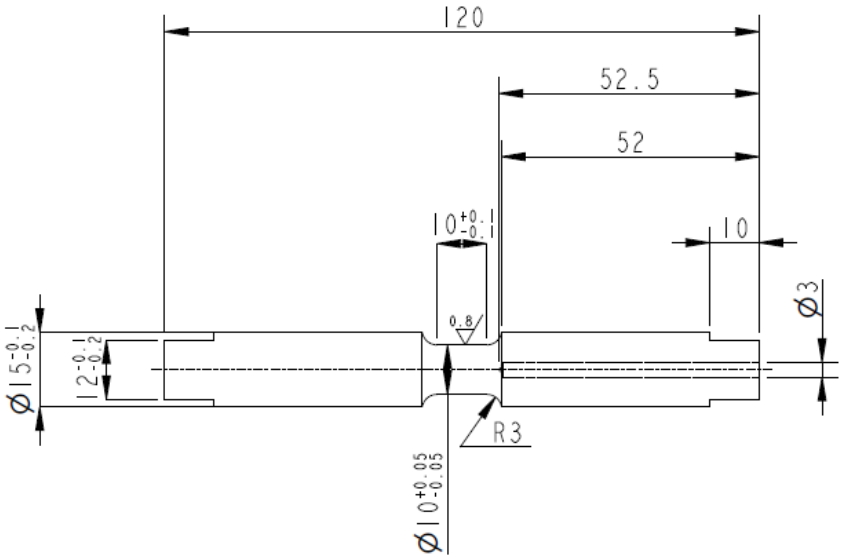

Fig. 1. Geometry of the solid cylindrical specimen used for hot torsion tests. The gauge section has a diameter of 10 mm and includes an axial hole (Ø3 mm, length 52.5 mm) for thermocouple placement, enabling accurate temperature monitoring during deformation.

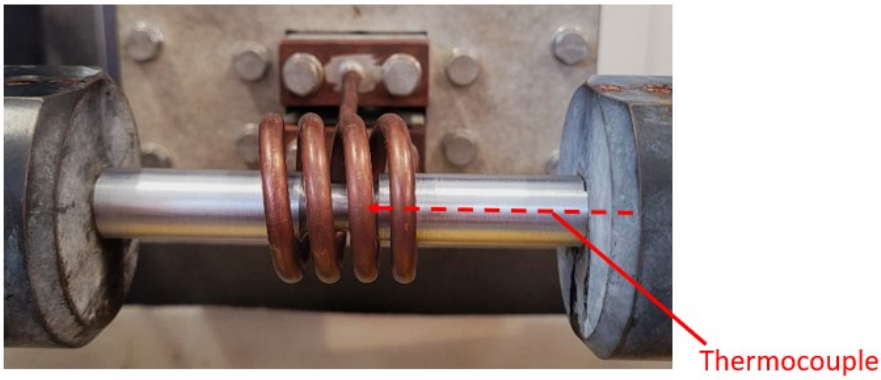

Fig. 2. Experimental setup for specimen heating using an induction copper coil. The thermocouple is positioned inside the axial hole near the gauge section, providing real-time temperature feedback for PID-controlled thermal regulation during torsion testing.

During the torsion test, the machine outputs the applied torque on the specimen [N·mm] and the corresponding angle of rotation [radians]. These data were analyzed using the Fields–Backofen model [6] to calculate the shear strain γ and the corresponding shear stress τ [MPa]. Using the Fields–Backofen model, it is therefore possible to obtain the strain, stress, and strain rate at the outer surface of the specimen, as described by Eq. 1, Eq. 2, and Eq. 3.

$$\gamma = \frac{R\,\theta}{L}\,, \qquad \text{Eq. (1)}$$

$$\dot{\gamma} = \frac{R\,\dot{\theta}}{L}\,, \qquad \text{Eq. (2)}$$

$$\tau = \frac{M}{2\,\pi\,R^3}(3 + n + m)\,, \qquad \text{Eq. (3)}$$

Where M is the applied torque expressed in N·mm, L is the gauge length of the specimen (10 mm), and R is the specimen radius (5 mm), as shown in Fig. 1. The parameter n represents the strain-

hardening coefficient (the instantaneous slope of logM versus logθ, as defined in Eq. 4), while m denotes the strain-rate sensitivity coefficient (the slope of logM versus log$\dot{\theta}$ at fixed θ, as defined in Eq. 5).

$$n = \left.\frac{\partial \log M}{\partial \log \theta}\right|_{\dot{\theta}}, \quad \text{Eq. (4)}$$

$$m = \left.\frac{\partial \log M}{\partial \log \dot{\theta}}\right|_{\theta}, \quad \text{Eq. (5)}$$

Several studies have shown that the coefficients associated with strain hardening and strain-rate sensitivity have a negligible influence on aluminum alloys when calculating flow stress, as their effect at high temperatures is significantly reduced [6]. For this reason, in this work the coefficients m and n were neglected, and the stress and strain were calculated using the von Mises formulation in accordance with Eq. 6 and Eq. 7.

$$\bar{\sigma} = \frac{M\, 3\sqrt{3}}{2\, \pi\, R^3}, \quad \text{Eq. (6)}$$

$$\bar{\varepsilon} = \frac{\gamma}{\sqrt{3}}. \quad \text{Eq. (7)}$$

Four different aluminum alloys were investigated: primary and recycled AA6082, recycled AA6061, and primary AA7108. Both the recycled AA6082 and AA6061 alloys were produced from 100% recycled scrap, supplied by industrial partners within the ZEvRA project. The chemical compositions of all four alloys are reported in Table 1.

As can be observed for the AA6082 alloy, there are several differences in chemical composition between the primary and the recycled material. For example, Fe increases from 0.19 wt% to 0.44 wt%, Cu from 0.001 wt% to 0.1 wt%, and Mn from 0.55 wt% to 0.9 wt%. An increase in Fe and Mn content would be expected to produce marginally higher flow stress peaks, particularly at low temperatures and high strain rates, along with a marginally reduced fracture strain, while overall maintaining a similar flow stress behavior. These are typical values for materials produced from 100% recycled scrap, for which a greater variability in chemical composition is to be expected.

AA6061 is a fully recycled alloy, the composition is presented as a range due to industrial confidentiality requirements imposed by the company. Despite its compositional heterogeneity, the Si and Mg contents remain within the standard ranges for 6xxx series alloys. The composition suggests good compatibility with hot-working processes.

As for AA7108, it is a primary alloy. The high Zn content (5.66 wt%) and the presence of Mg (0.88 wt%) reflect the typical chemistry of 7xxx series alloys. This composition results in higher flow stress peaks at low temperatures compared to the other alloys analyzed, but also in greater sensitivity to increasing temperature, with a marked reduction in flow stress at higher temperatures.

Table 1 Chemical composition (wt%) of the AA6061, AA6082 (primary and recycled), and AA7108 aluminum alloys. The AA6061 values are reported as ranges because the exact values are not disclosed due to industrial confidentiality. The balance to 100% is aluminum (Al).

Alloy	Fe	Si	Cu	Mn	Mg	Cr	Zn	Zr	Ti
AA6061	0.25-0.35	0.6-0.75	0.05-0.2	0.1-0.6	0.7-1	0.01-0.2	0.06-0.1	0.003-0.05	0.02-0.08
AA6082 Primary	0.19	0.94	0.001	0.55	0.64	0.15	0.01	0.003	0.007
AA6082 Recycled	0.44	0.9	0.1	0.9	0.66	0.15	0.07	0.002	0.018
AA7108	0.2	0.06	0.001	0.002	0.88	0.001	5.66	0.15	0.007

Each alloy was tested under a constant rotational speed and at a constant selected temperature throughout the duration of the test, with temperatures of 400, 450, 500, and 550 °C and strain rates of 0.01, 0.1, 1, and 10 s^{-1}. These conditions cover a typical range of strain, strain rate, and temperature values encountered in hot extrusion processes. From the torsion tests, flow stress curves in the σ–ε domain were obtained and analyzed. These curves are essential as input for material cards used in FEM numerical simulations. Subsequently, they were examined in the ln(σ)–ln(ε) domain, with ln(ε) on the horizontal axis and ln(σ) on the vertical axis, enabling a more accurate identification and study of the regions associated with softening through linear regression.
The peak was defined as the maximum value of σ reached during the test. To analyze post-peak softening, two regions of the flow stress curve were considered, and a linear regression was performed for each region, which are defined as:

- Initial softening tangent: defined as the slope resulting from a linear regression in the ln(σ)-ln(ε) domain: $a = \frac{d\ln(\sigma)}{d\ln(\varepsilon)}$, calculated over the first 30% of the experimental data points remaining after the peak flow stress, $\sigma_{peak;}$
- Final softening tangent: defined as the slope resulting from a linear regression in the ln(σ)-ln(ε) domain: $b = \frac{d\ln(\sigma)}{d\ln(\varepsilon)}$, calculated over the last 30% of the experimental data points remaining after the peak flow stress, $\sigma_{peak.}$

The slope, $a = \frac{d\ln(\sigma)}{d\ln(\varepsilon)}$ and $b = \frac{d\ln(\sigma)}{d\ln(\varepsilon)}$, and angle, $\theta = arctan(a)$ *and* $\beta = arctan(b)$ (degrees), quantify intensity and geometry of softening. Negative values denote softening.

Results

Flow stress curves. As previously mentioned, the hot torsion tests were conducted at temperatures of 400 °C, 450 °C, 500 °C, and 550 °C, and at strain rates of 0.01 s^{-1}, 0.1 s^{-1}, 1 s^{-1}, and 10 s^{-1}, for a total of sixteen distinct processing conditions, with two tests performed for each condition. The plots in Figs. 3–6 show the experimental results for the different alloys, presented as equivalent stress [MPa] versus equivalent strain curves. In each figure, the flow stress curves are grouped by temperature, with purple curves representing tests at 10 s^{-1}, orange curves at 1 s^{-1}, blue curves at 0.1 s^{-1}, and green curves at 0.01 s^{-1}. The flow stress curves exhibit the typical behavior observed in many aluminum alloys, characterized by a peak at low strain followed by a softening stage. The tests were terminated upon specimen fracture.

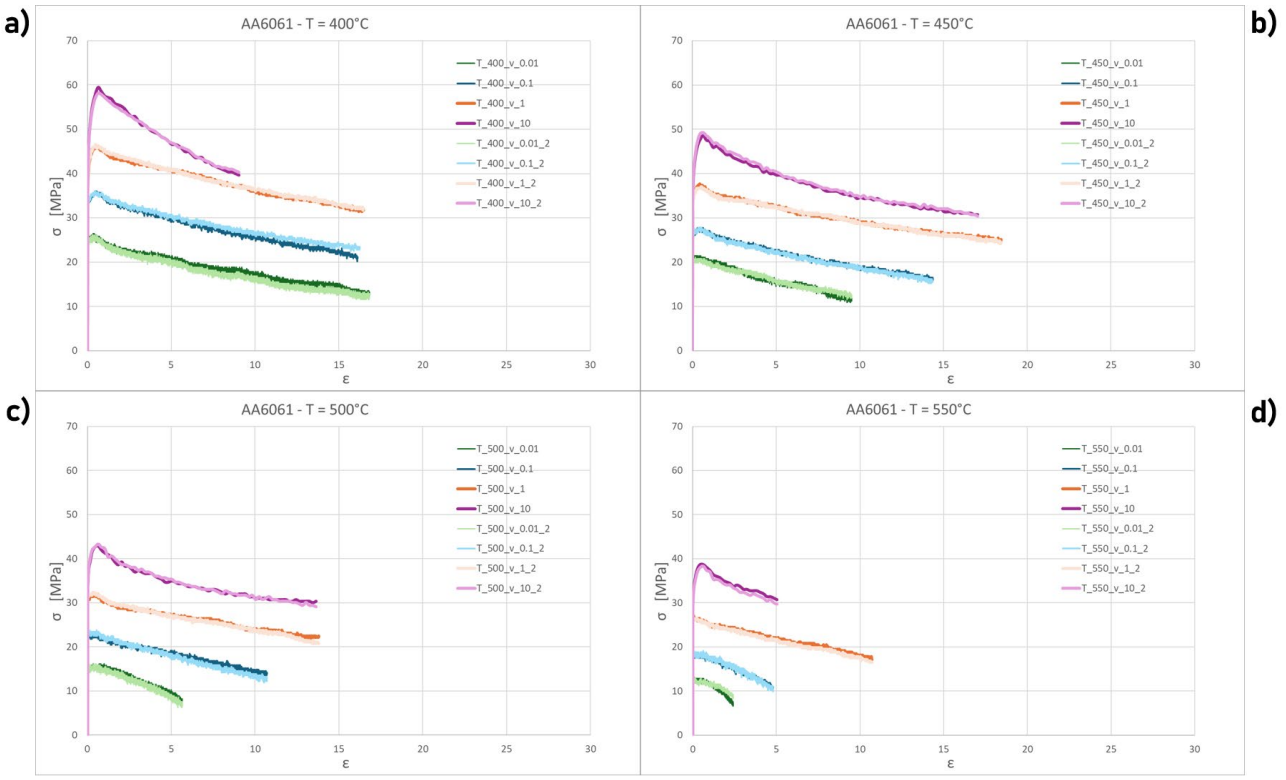

Fig. 3 Flow stress curves of AA6061 alloy obtained from hot torsion tests at different temperatures (400–550 °C) and strain rates (10, 1, 0.1, and 0.01 s^{-1}).

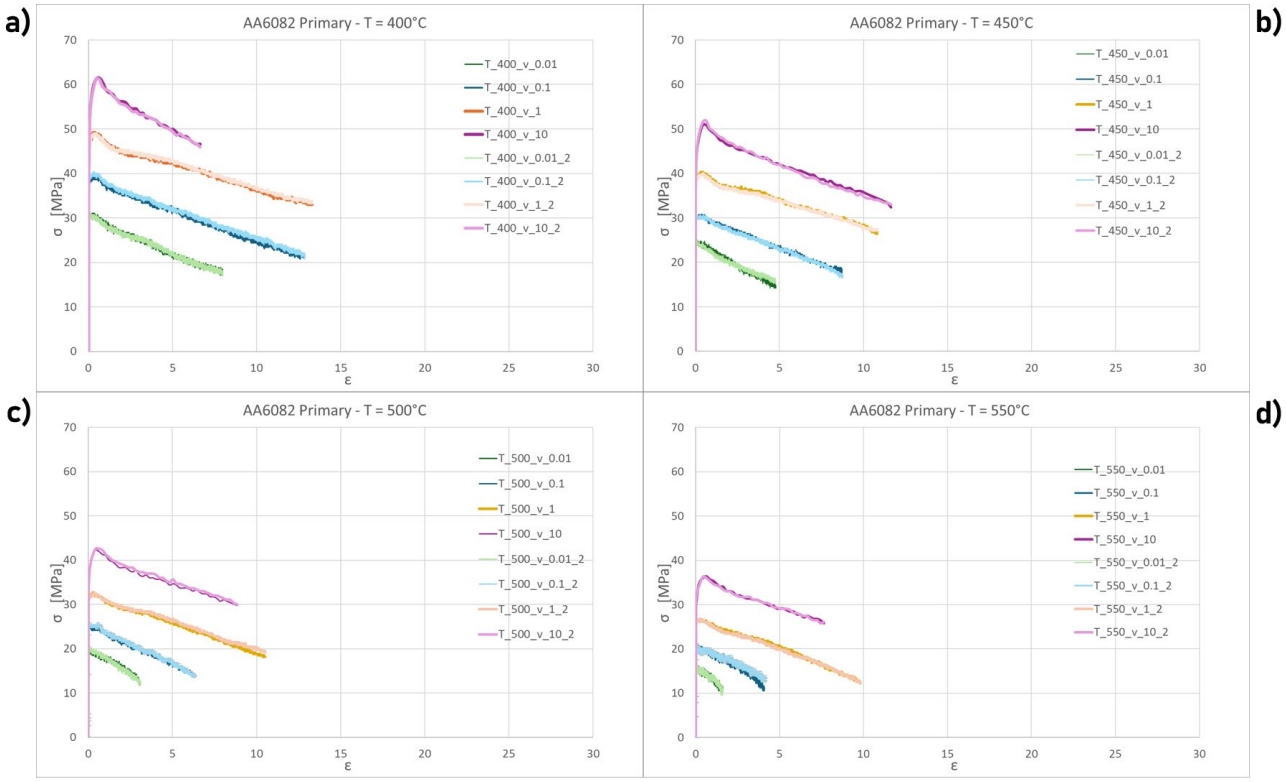

Fig. 4 Flow stress curves of AA6082 Primary alloy obtained from hot torsion tests at different temperatures (400–550 °C) and strain rates (10, 1, 0.1, and 0.01 s^{-1}).

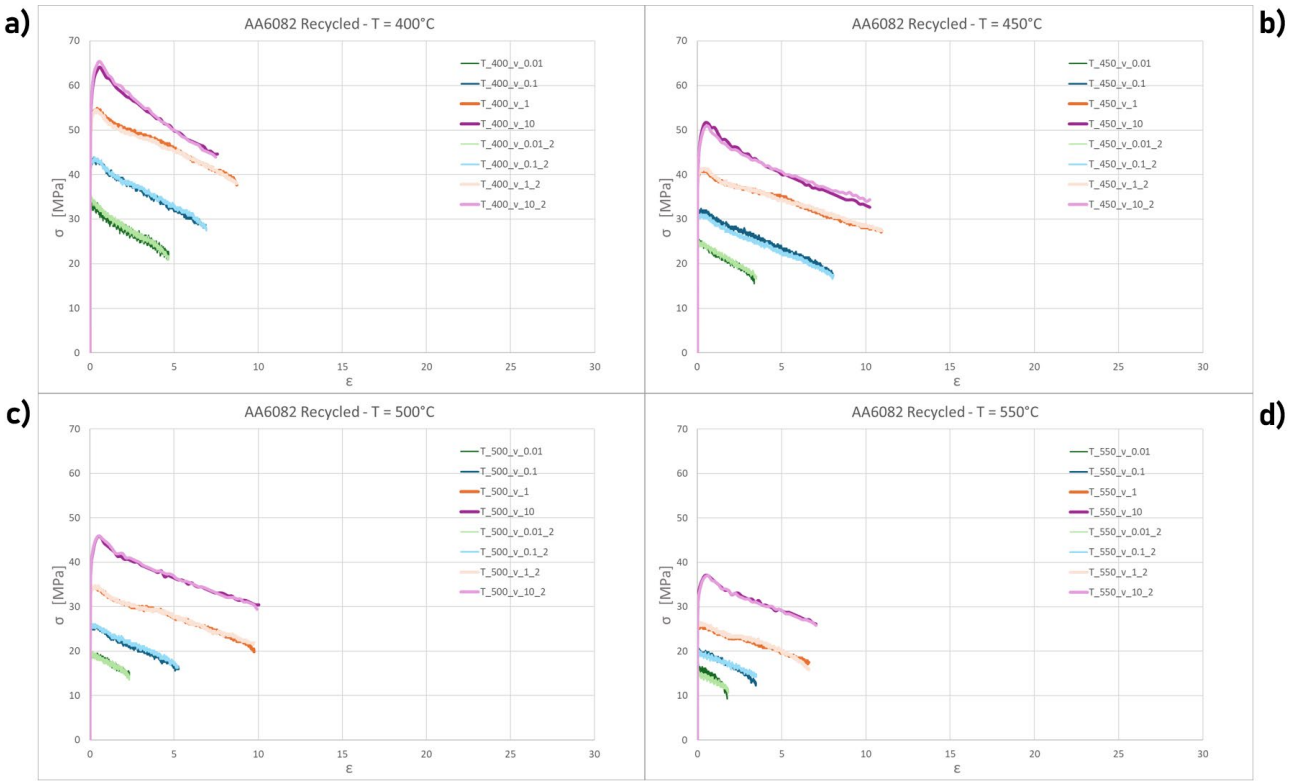

Fig. 5 Flow stress curves of AA6082 Recycled alloy obtained from hot torsion tests at different temperatures (400–550 °C) and strain rates (10, 1, 0.1, and 0.01 s^{-1}).

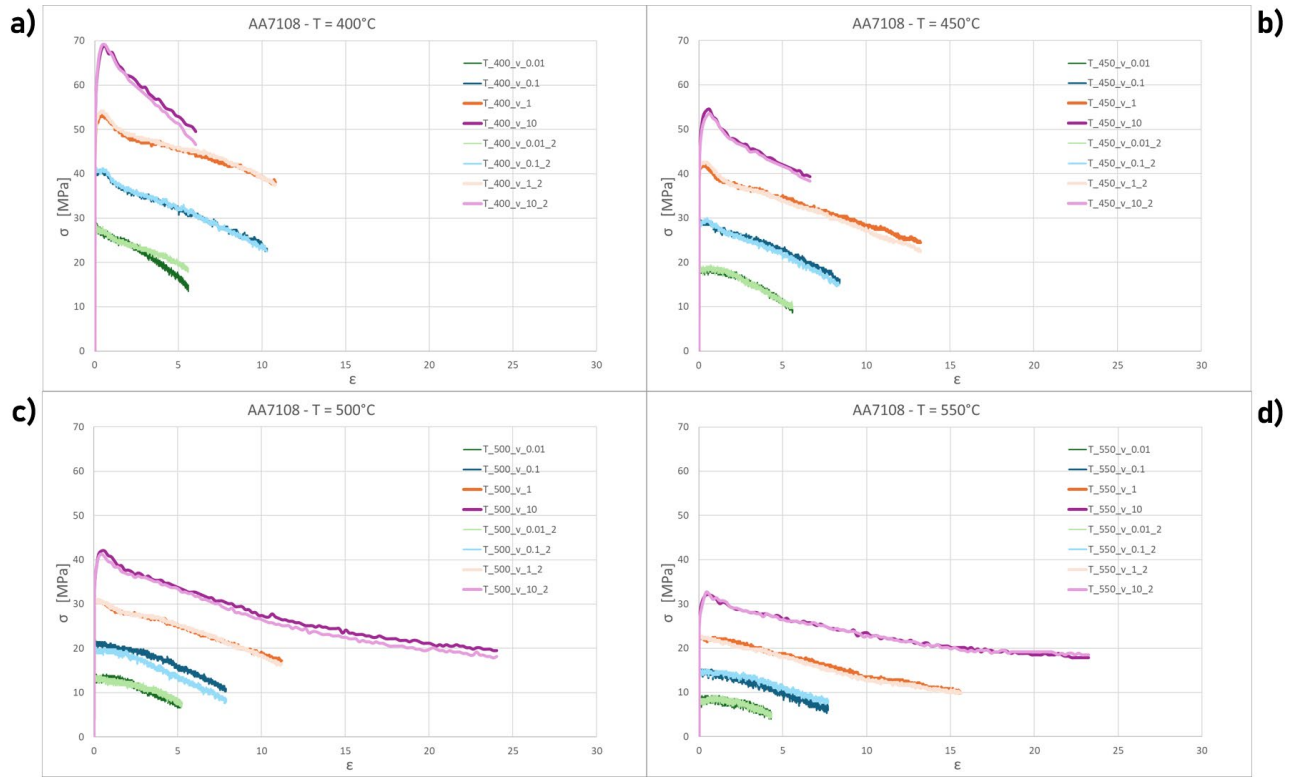

Fig. 6 Flow stress curves of AA7108 alloy obtained from hot torsion tests at different temperatures (400–550 °C) and strain rates (10, 1, 0.1, and 0.01 s^{-1}).

Peak Behavior: σ_{peak} and ε_{peak} vs. Temperature. From this point onward, the analysis of the curves was performed in the ln(σ)–ln(ε) domain, as this representation allows for a clearer assessment of the alloy's mechanical behavior, particularly at very low strain levels. For each combination of temperature and strain rate, two hot torsion tests were performed. In all cases, the results showed

excellent repeatability, with differences below 5% across all regions of the flow stress curve. Therefore, only the curve from the first test was considered in the subsequent analyses.
The maximum value of σ_{peak} in the flow stress curve and the corresponding ε_{peak} provide important information on the onset of the dynamic softening mechanisms of the alloys during hot torsion, namely the stress reduction due to dynamic recovery and/or recrystallization. For all alloys and strain rates, the peak flow stress σ_{peak} decreases systematically with increasing temperature, demonstrating the progressive reduction in the material's flow resistance due to thermal activation. This effect is associated with enhanced dislocation motion and recovery processes, defined as the thermally activated rearrangement and reduction in dislocation density, leading to a decrease in the stored deformation energy, as evidenced by the data reported in Fig. 7 and Table 2.
Fig. 7 shows the curves for alloy AA6061, with (a) corresponding to a strain rate of 0.01 s^{-1}, (b) to 0.1 s^{-1}, (c) to 1 s^{-1}, and (d) to 10 s^{-1}. The blue curves represent tests at 400 °C, orange at 450 °C, green at 500 °C, and red at 550 °C. Each curve includes a marker indicating the position of σ_{peak} and ε_{peak}, whose values are listed in the legend of each graph.

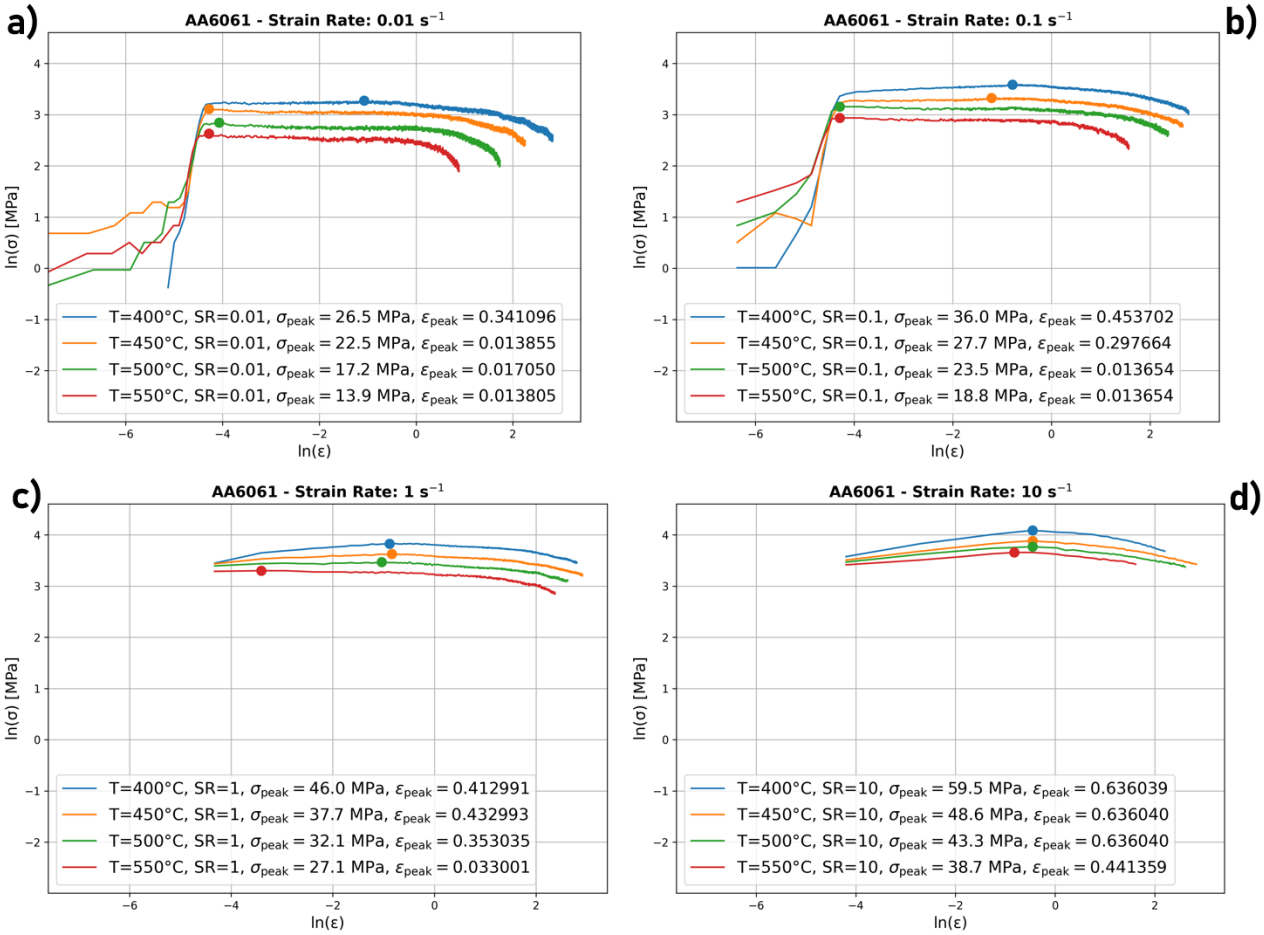

Fig. 7 Hot torsion flow curves for AA6061 alloy in the lnσ–lnε domain at different temperatures (400–550 °C) and strain rates (0.01 (a), 0.1 (b), 1 (c), 10 s^{-1} (d)). Symbols indicate peak stress (σ_{peak}) and corresponding strain (ε_{peak}). Post-peak softening behavior is evident, with thermal softening dominating at low strain rates and strain-rate hardening prevailing at high strain rates.

For clarity and space efficiency, the analysis of the values was continued in a table that also includes the other three alloys. Table 2 shows: (a) AA6061, (b) AA6082 Primary, (c) AA6082 Recycled, and (d) AA7108. Each sub-table contains three columns: test conditions (temperature and strain rate), the corresponding σ_{peak} value, and the corresponding ε_{peak} value. The list is organized into blocks, where orange indicates tests at 400 °C, blue at 450 °C, green at 500 °C, and purple at 550 °C.

Over the entire temperature range investigated (400 °C to 550 °C), the peak flow stress σ_{peak} is reduced by approximately 35% to 54%, starting from the highest value at 400 °C and gradually decreasing toward 550 °C, depending on the alloy and strain rate.

Table 2 Peak flow stress (σ_{peak}) and corresponding peak strain (ε_{peak}) obtained from hot torsion tests for AA6061 (a), AA6082 (Primary (b) and Recycled (c)), and AA7108 (d) alloys at different deformation temperatures and strain rates.

a)

AA6061	σ_{peak} [MPa]	ε_{peak}
T=400°C; SR=0.01 s^{-1}	26.5	0.34
T=400°C; SR=0.1 s^{-1}	36.0	0.45
T=400°C; SR=1 s^{-1}	46.0	0.41
T=400°C; SR=10 s^{-1}	59.5	0.64
T=450°C; SR=0.01 s^{-1}	22.5	0.01
T=450°C; SR=0.1 s^{-1}	27.7	0.30
T=450°C; SR=1 s^{-1}	37.7	0.43
T=450°C; SR=10 s^{-1}	48.6	0.64
T=500°C; SR=0.01 s^{-1}	17.2	0.02
T=500°C; SR=0.1 s^{-1}	23.5	0.01
T=500°C; SR=1 s^{-1}	32.1	0.35
T=500°C; SR=10 s^{-1}	43.3	0.64
T=550°C; SR=0.01 s^{-1}	13.9	0.01
T=550°C; SR=0.1 s^{-1}	18.8	0.01
T=550°C; SR=1 s^{-1}	27.1	0.03
T=550°C; SR=10 s^{-1}	38.7	0.44

b)

AA6082 Primary	σ_{peak} [MPa]	ε_{peak}
T=400°C; SR=0.01 s^{-1}	31.1	0.10
T=400°C; SR=0.1 s^{-1}	39.7	0.35
T=400°C; SR=1 s^{-1}	49.2	0.27
T=400°C; SR=10 s^{-1}	61.5	0.64
T=450°C; SR=0.01 s^{-1}	25.1	0.02
T=450°C; SR=0.1 s^{-1}	30.7	0.20
T=450°C; SR=1 s^{-1}	40.3	0.31
T=450°C; SR=10 s^{-1}	50.9	0.44
T=500°C; SR=0.01 s^{-1}	20.8	0.01
T=500°C; SR=0.1 s^{-1}	26.1	0.02
T=500°C; SR=1 s^{-1}	32.7	0.27
T=500°C; SR=10 s^{-1}	42.3	0.44
T=550°C; SR=0.01 s^{-1}	16.5	0.04
T=550°C; SR=0.1 s^{-1}	20.5	0.01
T=550°C; SR=1 s^{-1}	26.7	0.11
T=550°C; SR=10 s^{-1}	36.4	0.64

c)

AA6082 Recycled	σ_{peak} [MPa]	ε_{peak}
T=400°C; SR=0.01 s^{-1}	34.4	0.06
T=400°C; SR=0.1 s^{-1}	43.9	0.23
T=400°C; SR=1 s^{-1}	54.9	0.43
T=400°C; SR=10 s^{-1}	64.1	0.58
T=450°C; SR=0.01 s^{-1}	25.4	0.08
T=450°C; SR=0.1 s^{-1}	32.4	0.22
T=450°C; SR=1 s^{-1}	41.3	0.31
T=450°C; SR=10 s^{-1}	51.6	0.44
T=500°C; SR=0.01 s^{-1}	20.2	0.02
T=500°C; SR=0.1 s^{-1}	26.1	0.08
T=500°C; SR=1 s^{-1}	34.7	0.29
T=500°C; SR=10 s^{-1}	45.6	0.44
T=550°C; SR=0.01 s^{-1}	15.9	0.01
T=550°C; SR=0.1 s^{-1}	20.8	0.06
T=550°C; SR=1 s^{-1}	25.8	0.03
T=550°C; SR=10 s^{-1}	37.0	0.44

d)

AA7108	σ_{peak} [MPa]	ε_{peak}
T=400°C; SR=0.01 s^{-1}	29.1	0.07
T=400°C; SR=0.1 s^{-1}	41.0	0.32
T=400°C; SR=1 s^{-1}	53.5	0.43
T=400°C; SR=10 s^{-1}	68.7	0.64
T=450°C; SR=0.01 s^{-1}	19.5	0.01
T=450°C; SR=0.1 s^{-1}	29.8	0.02
T=450°C; SR=1 s^{-1}	42.0	0.23
T=450°C; SR=10 s^{-1}	54.5	0.64
T=500°C; SR=0.01 s^{-1}	14.5	0.01
T=500°C; SR=0.1 s^{-1}	22.5	0.01
T=500°C; SR=1 s^{-1}	31.1	0.25
T=500°C; SR=10 s^{-1}	42.0	0.44
T=550°C; SR=0.01 s^{-1}	9.2	0.03
T=550°C; SR=0.1 s^{-1}	15.5	0.01
T=550°C; SR=1 s^{-1}	22.8	0.09
T=550°C; SR=10 s^{-1}	32.1	0.44

As hypothesized based on the slight difference in chemical composition between AA6082 Primary and Recycled, the Recycled variant exhibits marginally higher σ_{peak} values, particularly at lower temperatures (400 °C and 450 °C) and higher strain rates (1 s^{-1} and 10 s^{-1}). However, the differences remain overall within an acceptable range. Moreover, looking at the trend at a constant strain rate, AA6082 Recycled shows a greater decrease in σ_{peak} with increasing temperature compared to the Primary alloy, as shown in Table 2.

Switching to AA6061, this alloy exhibits a systematic reduction in σ_{peak} with increasing temperature, decreasing from 26.55–59.5 MPa at 400 °C to 13.9–38.7 MPa at 550 °C, confirming the strong thermal softening typical of 6xxx-series alloys. The resistance to deformation consistently increases

with strain rate: raising the strain rate from 0.01 s^{-1} to 10 s^{-1} always results in a significant increase in σ_{peak}, shown in Fig.7 and Table 2.
The alloy with the strongest temperature dependence is 7108, which shows a consistent decrease from 400 °C to 550 °C across all strain rates. It starts from relatively high values (from 29 to 69 MPa at 400 °C) and drops to around 9–32 MPa at 550 °C, confirming the pronounced thermal softening typical of 7xxx-series alloys containing Zn and Mg. At a given temperature, increasing the strain rate from 0.01 s^{-1} to 10 s^{-1} always results in a marked increase in deformation resistance, indicating a strong strain-rate sensitivity of the alloy (Table 2).
In contrast, the strain-related peak parameter, ε_{peak}, exhibits a stronger dependence on strain rate than on temperature. At low strain rates (0.01–0.1 s^{-1}), ε_{peak} decreases markedly at intermediate and high temperatures, falling by about one order of magnitude, which indicates that the maximum flow stress is reached at very small strains (Fig.7, Table 2). At a strain rate of 10 s^{-1}, ε_peak remains high and only weakly dependent on temperature, forming a plateau generally in the strain range between 0.44 and 0.64.
Regarding AA6082, the Recycled alloy exhibits ε_{peak} values very similar to those of the Primary alloy across the entire range of temperatures and strain rates. Differences between the two alloys are small and non-systematic. In general, both alloys follow the same trend. Low ε_{peak} is observed at low strain rates (0.01 and 0.1 s^{-1}) from 450 °C onward, indicating early recrystallization. High, stable ε_{peak} (in the range 0.44–0.64) is seen at 10 s^{-1}, suggesting that high strain rates moderately inhibit the dynamic recrystallization, as shown in Table 2.
The same trend can also be observed for AA6061 and AA7108, as shown in Table 2.
In summary, temperature primarily influences the value of σ_{peak}, whereas strain rate mainly affects the strain at which the peak occurs, corresponding to the initial softening behavior.

Initial Softening (first 30% post-peak). Initial softening is defined as the early post-peak portion of the flow stress curve, where the slope of the tangent indicates a decrease in stress due to the activation of dynamic softening mechanisms, such as dynamic recovery and the possible onset of dynamic recrystallization. In this case, the analysis was focused on the effect of strain rate.
Accordingly, Fig. 8 presents the results obtained at a strain rate of 0.01 s^{-1}. The figure is divided into four subplots: (a) AA6061, (b) AA6082 Primary, (c) AA6082 Recycled, and (d) AA7108. The blue curves correspond to T = 400 °C, the orange curves to T = 450 °C, the green curves to T = 500 °C, and the red curves to T = 550 °C. The initial softening tangent is indicated on the curves by a dark-gray dashed line, and the corresponding values are reported in the table, where *a* denotes the slope ($a = \frac{d\ln(\sigma)}{d\ln(\varepsilon)}$) and θ is the associated angle ($\theta = arctan(a)$), expressed in degrees.
In general, at low strain rates, between 0.01 s^{-1} and 0.1 s^{-1}, the negative slope of the initial softening tangent is more pronounced at 400 °C and progressively decreases with increasing temperature, resulting in a gradual reduction in slope up to 550 °C, where the curve tends to flatten a as shown in Fig.8 and Tab.2.
At a strain rate of 0.01 s^{-1}, AA6082 alloys exhibit a decrease in the slope angle from 400°C to 550°C. AA6082 shifts from -3.8° to -1.7°, and AA6082 Recyled follows a similar trend, shifting from -3.0° to -1.6°.
AA6061 exhibits a decrease in the slope angle from −5.1° to −1.1°, corresponding to an approximate 80% reduction. AA7108 shows a positive softening angle, suggesting that, in the post-peak region, dynamic recovery and dynamic recrystallization mechanisms become dominant. These processes reduce damage accumulation and stabilize the mechanical behavior of the alloy, leading to an, only apparent, recovery in flow stress. Overall, the initial tangent decrease in value almost monotonically with temperature, producing a clear reduction in severity and, in some cases, temporary stabilization.

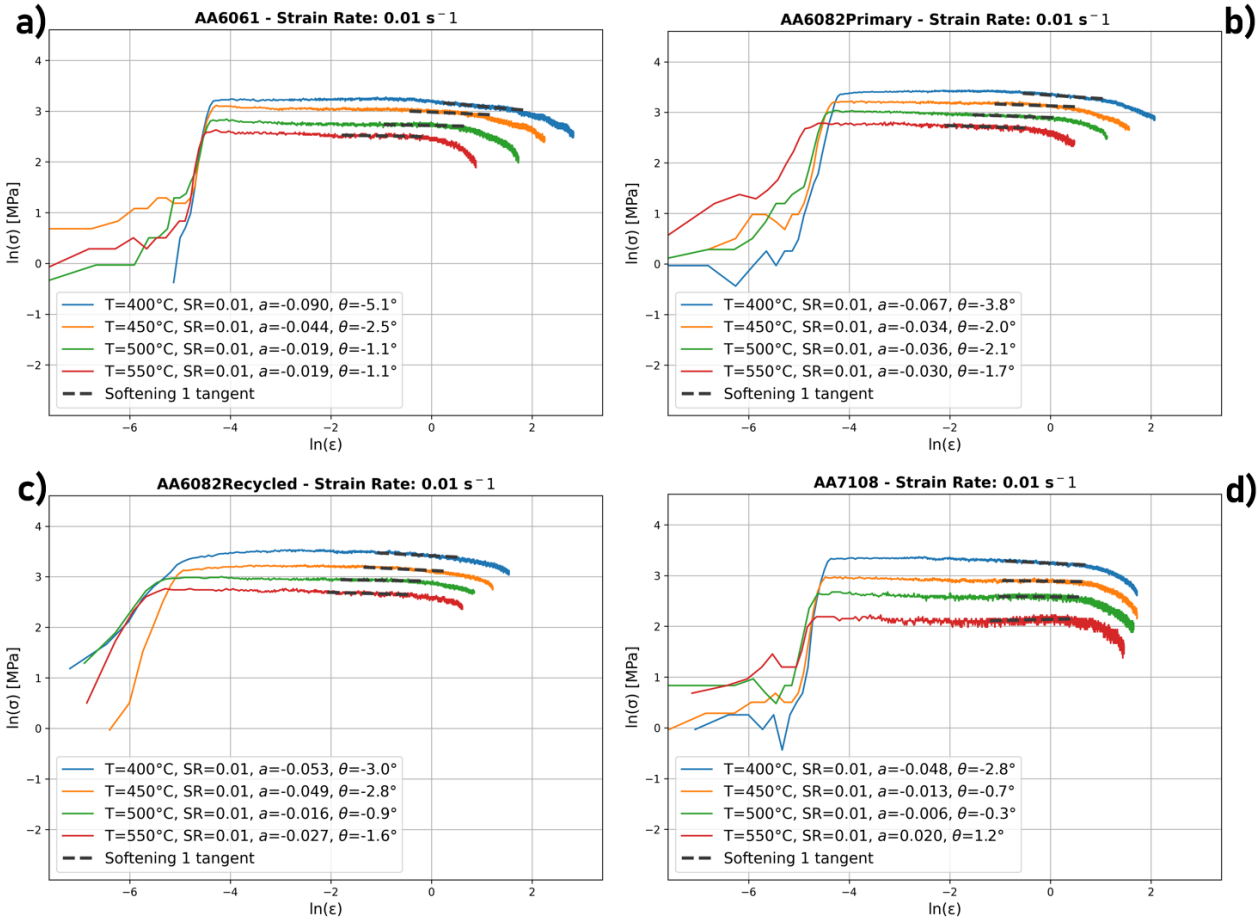

Fig. 8 Initial softening behavior (first 30% of post-peak data) for AA6061 (a), AA6082 Primary (b), AA6082 Recycled (c), and AA7108 (d) alloys at a strain rate of 0.01 s^{-1}. Linear regressions highlight the initial softening tangent (black dashed lines), with slope a and angle θ reported for each temperature. Increasing temperature reduces the severity of early post-peak softening.

Regarding Table 3, the same organizational approach adopted for Fig. 8 was followed. The table is divided into subtables according to strain rate: (a) 0.01 s^{-1}, (b) 0.1 s^{-1}, (c) 1 s^{-1}, and (d) 10 s^{-1}. Each subtable consists of three columns: the first reports the investigated alloy together with the corresponding temperature, the second lists the value of the initial softening slope a, and the third provides the corresponding initial softening angle θ, expressed in degrees. For clarity, the data are further grouped by alloy: AA6061 is highlighted in orange, AA6082 Primary in light blue, AA6082 Recycled in green, and AA7108 in purple.

Across the three other analyzed strain rates, AA6082 Recycled closely follows the trend of AA6082 Primary, with limited differences over the investigated temperature range. Specifically, the Recycled alloy exhibits a marginally increased slope than the Primary at 450°C and 0.1 s^{-1}, whereas it shows a slightly lower slope at 550°C and 1 s^{-1}. At 10 s^{-1}, the differences in initial softening between the two alloys remain very moderate, reaching identical values at 550°C. Overall, the two alloys display very similar behavior in terms of initial softening.

Regarding AA6061, at 0.1 s^{-1} initial softening decreases monotonically, from –4.7° to –1.4°. At 1 s^{-1}, the decrease is noticeable only at 550 °C, while at 10 s^{-1} the slopes remain practically constant across the different temperatures.

Moving on to AA7108, the softening decreases with temperature, from –4.7° to –1.8° at a strain rate of 0.1 s^{-1}. At 1 s^{-1}, the values are moderate and almost constant, with a noticeable decrease again at 550 °C. At 10 s^{-1}, the softening is more pronounced in terms of slope (negative angle), but the values remain practically constant across the temperature range.

On average, the values of the *initial softening slope a* at a strain rate of 0.1 s^{-1} are slightly higher in magnitude (i.e., more negative), with only a few exceptions. However, the trend closely mirrors that observed for the curves at 0.01 s^{-1}, as presented in Table 3. At a strain rate of 1 s^{-1}, the post-peak

initial softening exhibits values that are less dependent on temperature, with trends that are not always monotonic (Table 3). In some alloys, the slope of the tangent does not decrease systematically with increasing temperature, as observed at strain rates of 0.01 and 0.1 s^{-1}.
Specifically, for AA6082 (both recycled and primary), the maximum negative slopes were recorded at 500°C; for AA6061 at 450°C; whereas for AA7108 the behavior remained monotonic. These data suggest that, unlike at strain rates of 0.01 and 0.1 s^{-1}, the high rotational speed begins to counteract recovery and dynamic recrystallization phenomena, reducing the influence of temperature. In this case, temperature therefore plays a more secondary and nonlinear role in determining the initial softening slope (Table 3). At the highest strain rate of 10 s^{-1}, the tangent shows only minor differences across temperatures, remaining practically insensitive to temperature changes (Table 3). For all alloys, the slope of the tangent at a strain rate of 10 s^{-1} is higher than that observed at lower strain rates, with only slight variations across temperature levels and, in some cases, a slight intensification at intermediate temperatures. These values suggest, consistent with the results at 1 s^{-1}, that at higher deformation rates the mechanisms of recovery and recrystallization have a much smaller influence on the mechanical behavior of the material.

Table 3 Initial post-peak softening characteristics in terms of local tangent and slope angle in lnσ–lnε coordinates for AA6061, AA6082 (Primary and Recycled), and AA7108 alloys tested in hot torsion at different temperatures(400°C to 550°C) and strain rates (0.01 (a), 0.1 (b), 1 (c) and 0.01 s^{-1} (d)).

a)

Strain Rate = 0.01s^{-1}	Initial Softening (a)	Initial Softening (θ [°])
AA6061_400°C	-0.090	-5.1
AA6061_450°C	-0.043	-2.5
AA6061_500°C	-0.018	-1.0
AA6061_550°C	-0.019	-1.1
AA6082Primary_400°C	-0.067	-3.8
AA6082Primary_450°C	-0.034	-2.0
AA6082Primary_500°C	-0.036	-2.1
AA6082Primary_550°C	-0.030	-1.7
AA6082Recycled_400°C	-0.053	-3.0
AA6082Recycled_450°C	-0.049	-2.8
AA6082Recycled_500°C	-0.016	-0.9
AA6082Recycled_550°C	-0.027	-1.6
AA7108_400°C	-0.048	-2.8
AA7108_450°C	-0.013	-0.7
AA7108_500°C	-0.006	-0.3
AA7108_550°C	0.020	1.2

b)

Strain Rate = 0.1s^{-1}	Initial Softening (a)	Initial Softening (θ [°])
AA6061_400°C	-0.083	-4.7
AA6061_450°C	-0.078	-4.5
AA6061_500°C	-0.041	-2.3
AA6061_550°C	-0.025	-1.4
AA6082Primary_400°C	-0.080	-4.6
AA6082Primary_450°C	-0.060	-3.4
AA6082Primary_500°C	-0.046	-2.6
AA6082Primary_550°C	-0.025	-1.4
AA6082Recycled_400°C	-0.067	-3.8
AA6082Recycled_450°C	-0.074	-4.3
AA6082Recycled_500°C	-0.050	-2.9
AA6082Recycled_550°C	-0.028	-1.6
AA7108_400°C	-0.083	-4.7
AA7108_450°C	-0.038	-2.2
AA7108_500°C	-0.026	-1.5
AA7108_550°C	-0.032	-1.8

c)

Strain Rate = 1s^{-1}	Initial Softening (a)	Initial Softening (θ [°])
AA6061_400°C	-0.054	-3.1
AA6061_450°C	-0.063	-3.6
AA6061_500°C	-0.062	-3.5
AA6061_550°C	-0.040	-2.3
AA6082Primary_400°C	-0.058	-3.3
AA6082Primary_450°C	-0.054	-3.1
AA6082Primary_500°C	-0.070	-4.0
AA6082Primary_550°C	-0.062	-3.6
AA6082Recycled_400°C	-0.060	-3.4
AA6082Recycled_450°C	-0.058	-3.3
AA6082Recycled_500°C	-0.074	-4.2
AA6082Recycled_550°C	-0.037	-2.1
AA7108_400°C	-0.074	-4.3
AA7108_450°C	-0.065	-3.7
AA7108_500°C	-0.059	-3.4
AA7108_550°C	-0.055	-3.2

d)

Strain Rate = 10s^{-1}	Initial Softening (a)	Initial Softening (θ [°])
AA6061_400°C	-0.090	-5.1
AA6061_450°C	-0.107	-6.1
AA6061_500°C	-0.102	-5.9
AA6061_550°C	-0.090	-5.2
AA6082Primary_400°C	-0.083	-4.7
AA6082Primary_450°C	-0.084	-4.8
AA6082Primary_500°C	-0.081	-4.7
AA6082Primary_550°C	-0.100	-5.7
AA6082Recycled_400°C	-0.092	-5.3
AA6082Recycled_450°C	-0.103	-5.9
AA6082Recycled_500°C	-0.093	-5.3
AA6082Recycled_550°C	-0.100	-5.7
AA7108_400°C	-0.098	-5.6
AA7108_450°C	-0.115	-6.6
AA7108_500°C	-0.125	-7.1
AA7108_550°C	-0.099	-5.7

Final Softening (last 30% post-peak). Final softening refers to the final portion of the post-peak curve, corresponding to the last 30% of the data following the maximum flow stress value. In this region, a pronounced increase in softening is observed, mainly due to microstructural degradation of the alloy induced by high strain levels.
In Fig. 9, following the same scheme used for the initial softening, the curves at a strain rate of 0.01 s^{-1} corresponding to the final softening are presented. The subplots show: (a) AA6061, (b) AA6082 Primary, (c) AA6082 Recycled, and (d) AA7108. The curves are colored according to temperature: blue for T = 400 °C, orange for 450 °C, green for 500 °C, and red for 550 °C. The

tangent resulting from the linear regression is indicated by a dashed purple line. The corresponding values of the tangent are listed in the legend of each subplot, with $b = \frac{d\ln(\sigma)}{d\ln(\varepsilon)}$, and β = arctan(b).

Regarding Table 4, following the same organization as Table 3, with the subtables arranged according to strain rate. Each subtable contains three columns: test temperature, the corresponding final softening slope b, and the corresponding final softening angle in degrees, β.

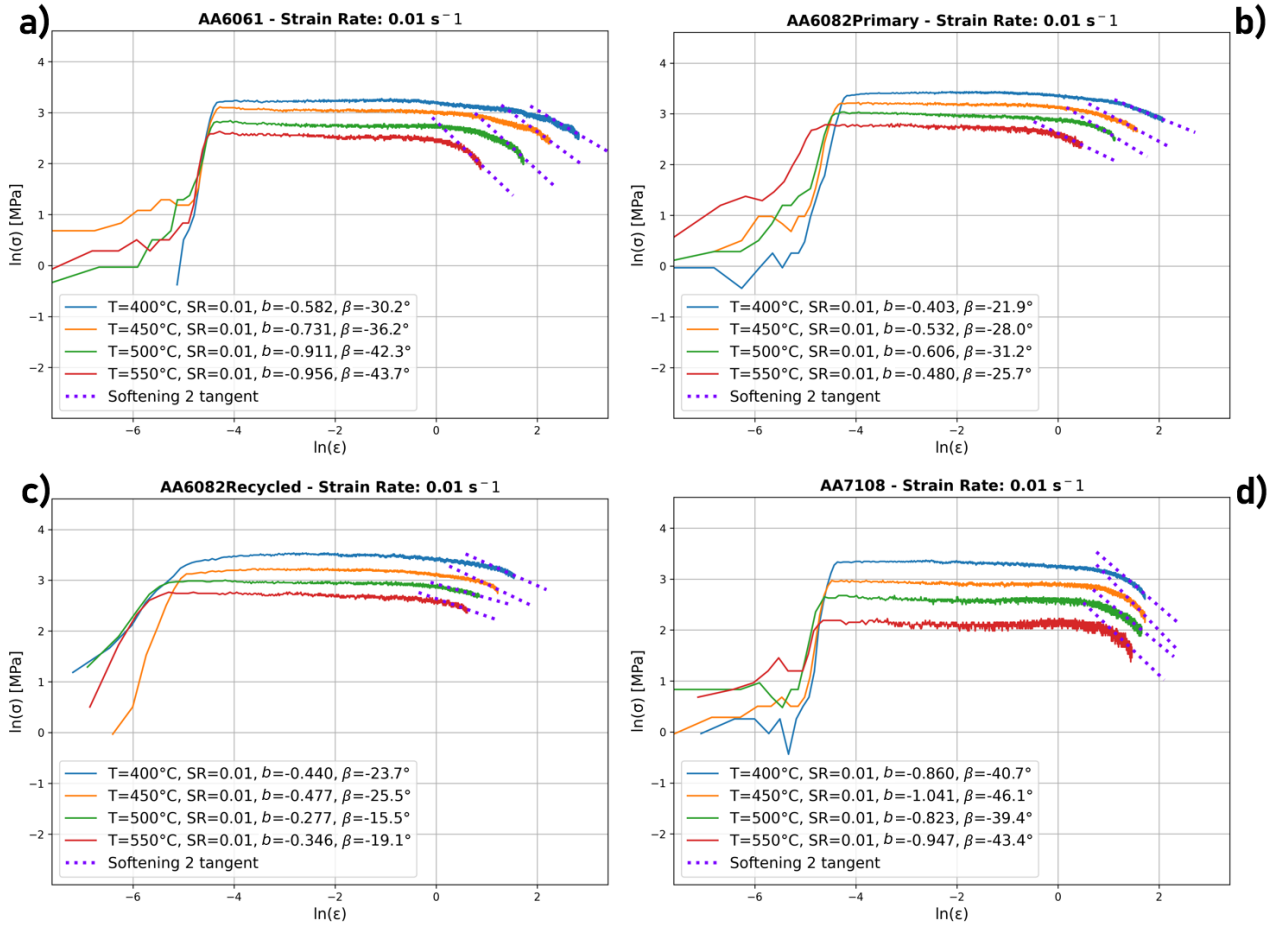

Fig. 9 Final softening behavior (last 30% post-peak) for AA6061 (a), AA6082 Primary (b), AA6082 Recycled (c), and AA7108 (d) alloys at a strain rate of 0.01 s^{-1}. Purple dashed lines indicate the final softening tangent, with slope b and angle β reported for each temperature.

At a strain rate of 0.01 s^{-1} the two AA6082 alloys exhibit very similar behavior between 400°C and 450°C, with comparable slope values. The most evident differences emerge at 500°C, where the Recycled alloy shows less pronounced softening compared to the Primary alloy. At 550 °C, the values of the tangent angle converge again, becoming closer to each other. However, for primary AA6082 the value at 550 °C remains higher than that observed at 400 °C, whereas for the recycled alloy the tangent angle decreases, reaching a lower value (still negative) compared to 400 °C. The recycled material displays only limited differences from the primary alloy, confirming a comparable thermomechanical response.

On average, for AA6061 and AA7108, the tangent associated with final softening increases in slope when moving from 400 °C to 550 °C. For AA6061, the trend is monotonic, whereas for AA7108 a peak occurs at 450 °C, followed by a decrease at 500 °C and then a rise again at 550 °C, reaching a value slightly higher than the tangent angle at 400 °C, as shown in Fig.9.

In this regime, the high levels of strain promote microstructural degradation mechanisms within the alloy, which are increasingly activated as temperature rises and prevail over dynamic recovery and dynamic recrystallization before complete specimen failure occurs. Consequently, in this region the tangent slope is significantly higher than that observed during the initial softening stage.

Table 4 Final post-peak softening characteristics, evaluated over the last 30% of the post-peak regime, in terms of local tangent and slope angle in lnσ–lnε coordinates for AA6061, AA6082 (Primary and Recycled), and AA7108 alloys tested in hot torsion at different temperatures (400°C to 550°C) and strain rates ((0.01 (a), 0.1 (b), 1 (c) and 0.01 s^{-1} (d)) .

a)

Strain Rate = 0.01s^{-1}	Final Softening (b)	Final Softening (β [°])
AA6061_400°C	-0.582	-30.2
AA6061_450°C	-0.729	-36.1
AA6061_500°C	-0.916	-42.5
AA6061_550°C	-0.958	-43.8
AA6082Primary_400°C	-0.403	-21.9
AA6082Primary_450°C	-0.532	-28.0
AA6082Primary_500°C	-0.606	-31.2
AA6082Primary_550°C	-0.480	-25.7
AA6082Recycled_400°C	-0.440	-23.7
AA6082Recycled_450°C	-0.477	-25.5
AA6082Recycled_500°C	-0.277	-15.5
AA6082Recycled_550°C	-0.346	-19.1
AA7108_400°C	-0.860	-40.7
AA7108_450°C	-1.041	-46.1
AA7108_500°C	-0.823	-39.4
AA7108_550°C	-0.947	-43.4

b)

Strain Rate = 0.1s^{-1}	Final Softening (b)	Final Softening (β [°])
AA6061_400°C	-0.399	-21.7
AA6061_450°C	-0.417	-22.6
AA6061_500°C	-0.481	-25.7
AA6061_550°C	-0.650	-33.0
AA6082Primary_400°C	-0.557	-29.1
AA6082Primary_450°C	-0.498	-26.5
AA6082Primary_500°C	-0.645	-32.8
AA6082Primary_550°C	-0.890	-41.7
AA6082Recycled_400°C	-0.412	-22.4
AA6082Recycled_450°C	-0.675	-34.0
AA6082Recycled_500°C	-0.479	-25.6
AA6082Recycled_550°C	-0.656	-33.2
AA7108_400°C	-0.561	-29.3
AA7108_450°C	-0.801	-38.7
AA7108_500°C	-0.991	-44.7
AA7108_550°C	-1.051	-46.4

c)

Strain Rate = 1s^{-1}	Final Softening (b)	Final Softening (β [°])
AA6061_400°C	-0.284	-15.9
AA6061_450°C	-0.259	-14.5
AA6061_500°C	-0.259	-14.5
AA6061_550°C	-0.431	-23.3
AA6082Primary_400°C	-0.323	-17.9
AA6082Primary_450°C	-0.414	-22.5
AA6082Primary_500°C	-0.633	-32.3
AA6082Primary_550°C	-0.919	-42.6
AA6082Recycled_400°C	-0.345	-19.1
AA6082Recycled_450°C	-0.337	-18.6
AA6082Recycled_500°C	-0.580	-30.1
AA6082Recycled_550°C	-0.436	-23.5
AA7108_400°C	-0.281	-15.7
AA7108_450°C	-0.503	-26.7
AA7108_500°C	-0.626	-32.1
AA7108_550°C	-0.760	-37.2

d)

Strain Rate = 10s^{-1}	Final Softening (b)	Final Softening (β [°])
AA6061_400°C	-0.318	-17.6
AA6061_450°C	-0.233	-13.1
AA6061_500°C	-0.212	-12.0
AA6061_550°C	-0.229	-12.9
AA6082Primary_400°C	-0.253	-14.2
AA6082Primary_450°C	-0.410	-22.3
AA6082Primary_500°C	-0.321	-17.8
AA6082Primary_550°C	-0.295	-16.4
AA6082Recycled_400°C	-0.287	-16.0
AA6082Recycled_450°C	-0.341	-18.8
AA6082Recycled_500°C	-0.314	-17.4
AA6082Recycled_550°C	-0.360	-19.8
AA7108_400°C	-0.320	-17.8
AA7108_450°C	-0.239	-13.4
AA7108_500°C	-0.406	-22.1
AA7108_550°C	-0.288	-16.0

Considering the strain rate of 0.1 s^{-1}, the overall trend is similar to that observed at 0.01 s^{-1}. For all alloys, an increase in the slope of the tangent is observed as the temperature rises from 400 °C to 550 °C. For AA6061, the increase in slope is monotonic with temperature, as also observed for AA7108. Returning to the comparison between the two AA6082 alloys, both exhibit the same temperature-dependent evolution across the three strain rates. At 0.1 and 1 s^{-1}, more noticeable differences emerge at higher temperatures, with the Primary alloy showing more pronounced final softening, particularly at 550°C. At 10 s^{-1}, the curves remain close over the entire temperature range, with smaller differences and nearly overlapping at 500°C. In general, the Recycled alloy again demonstrates behavior comparable to that of the Primary alloy.

Regarding the behavior of AA6061 and AA7108 at a strain rate of 1 s^{-1}, the alloys exhibit a generally monotonic trend, with the tangent slope decreasing as temperature increases. In this case, the behavior of the alloys at this strain rate is therefore strongly correlated with temperature, as represented in Table 4. Considering the curves obtained at a strain rate of 10 s^{-1}, the slopes of the final softening tangents are overall lower than those observed in the other tests. Also in this case, similarly to the initial softening stage, the curve behavior remains weakly dependent on temperature. The high deformation rate does not allow the development of diffuse damage processes as observed at lower strain rates, resulting in a less pronounced collapse of the curve prior to specimen failure.

Discussion

The analysis of hot torsion tests on AA6061, AA6082 (Primary and Recycled), and AA7108 shows a clear dependence of softening behavior on both temperature and strain rate. As a general trend, the initial softening tangent decreases in slope with increasing temperature, particularly at lower strain rates. In contrast, the final softening tangent increases as temperature rises, a trend that is also associated with the accumulation of damage in the alloy at high strain levels. The behaviors of the two regions, analyzed in the $\ln(\sigma)$–$\ln(\varepsilon)$ domain through linear regression of the curves over the first 30% and the last 30% of the data after the flow stress peak, are consistent with thermally activated mechanisms such as dynamic recovery (DRV) and continuous dynamic recrystallization (CDRX), which are widely documented in aluminum alloys subjected to hot plastic deformation [8–11]. EBSD and TEM studies on 7xxx alloys support these interpretations, showing that at elevated temperatures and during deformation there is a progressive increase in misorientation, an evolution of subgrains into high-angle grain boundaries (HAGBs), and the formation of equiaxed grains [8,9,16].

AA6061 Recycled also exhibited behavior very similar to that of the primary AA6061 alloys [11,12], with initial softening decreasing as temperature increases and final softening showing more pronounced slopes, particularly at strain rates of 0.1 s^{-1} and 1 s^{-1}. AA7108 exhibited final softening tangents with an increased slope at the lower strain rates (ranging from −39° to −47°), in agreement with the literature on Al–Zn–Mg–Cu alloys, where prolonged exposure at high temperature promotes recrystallization and leads to a reduction in material strength [15,18]. At low strain rates (0.01–0.1 s^{-1}), final softening intensifies with increasing temperature for all alloys, with AA7108 and the AA6082 alloys in particular following similar trends [5,11,14]. At 1 s^{-1}, thermal activation also amplifies the final tangent, with AA6082 Primary exhibiting the largest increase in slope, from −17.8° to −43.2° [7,12]. At 10 s^{-1}, the effect becomes more moderate and non-monotonic: AA7108 reaches a peak severity at 500 °C before attenuating, whereas AA6082 maintains a nearly linear trend even under high strain-rate conditions [7,12].

Focusing on the AA6082 alloys, as expected, an increase in Fe and Mn resulted in a slightly stronger and less ductile alloy. However, the effects were marginal and consistent with the literature and with prior expectations. Regarding the peak stress (σ_{peak}), the differences remained limited. They were more evident at low temperatures and high strain rates. In contrast, the peak strain (ε_{peak}) values were almost identical for the two alloys. This indicates similar recrystallization kinetics. The initial softening showed the same temperature dependence for both materials. The differences were minimal and not systematic. For the final softening stage, both alloys exhibited the same evolution with temperature and strain rate. Marginally more visible differences appeared only at high temperatures and low strain rates. In this regime, the primary alloy tended to show a slightly more pronounced softening. These results suggest that damage accumulation and continuous dynamic recrystallization are not adversely affected by the chemical composition differences in the recycled alloy. Overall, the recycled alloy shows performance comparable to that of the primary material. This confirms that the use of recycled alloys in no way compromises hot metal forming processes. It also supports their application in high-performance extrusion processes, from both a process sustainability and recycling perspective [3].

Conclusions

This study examines the hot deformation behavior of primary and secondary aluminum alloys through extensive mechanical characterization under typical industrial metal forming conditions. Analysis of flow stress curves in the $\ln(\sigma)$–$\ln(\varepsilon)$ domain, focusing on initial and final softening, highlights key thermomechanical features and their implications for process design and material circularity.

The main findings can be summarized as follows:

Temperature and strain rate effects on softening:

- During initial softening, the tangent slope decreases with increasing temperature at low strain rates (0.01–0.1 s^{-1}), indicating activation of dynamic recovery (DRV) and continuous dynamic recrystallization (CDRX). At higher strain rates (1 s^{-1} and 10 s^{-1}), this trend becomes negligible, as the rapid deformation suppresses recovery mechanisms;
- In the final softening stage, the tangent slope increases with increasing temperature at strain rates of 0.01–1 s^{-1}, due to microstructural degradation and damage accumulation. At 10 s^{-1}, softening remains moderate with little temperature dependence, reflecting the limited effect of thermally activated processes under rapid deformation.

Contribution of the study:

- This work provides a comparison of the flow stress curves between primary and recycled AA6082, with a particular focus on the initial and final softening regions, over a range of temperatures and strain rates commonly used in hot extrusion tests;
- While the detailed comparison focuses on AA6082, the study also presents the hot deformation behavior of recycled AA6061 and primary AA7108, providing valuable reference data for other widely used automotive aluminum alloys.

Comparison of primary and recycled AA6082:

- Recycled AA6082 exhibits softening behavior closely matching that of the primary alloy, supporting its potential use in industrial extrusion processes and circular production strategies.

Behavior of other alloys:

- AA6061 follows trends typical of 6xxx series alloys;
- AA7108 shows pronounced final softening at low strain rates, consistent with its higher temperature sensitivity and recrystallization behavior as reported for 7xxx series alloys.

Implications for FEM modeling:

- Incorporating these material characterizations into FEM material cards significantly improves simulation accuracy, further reducing prediction errors and enabling more precise design of the process digital twin;
- Torsion tests, performed over a wide range of strains, allow for precise characterization of the softening regions, providing extensive data that can be used in FEM material cards for model calibration and industrial process design.

Funding

This work was funded by the European Union's Horizon Europe research and innovation programme, under No. 101138034 as part of the project Zero Emission electric Vehicles enabled by haRmonised circularity (ZEvRA).

References

[1] V.K. Soo, J. Peeters, D. Paraskevas, P. Compston, M. Doolan, J.R. Duflou, Sustainable aluminium recycling of end-of-life products: a joining techniques perspective, J. Clean Prod. 178 (2018) 119–132.

[2] V.K. Soo, P. Compston, M. Doolan, Interaction between new car design and recycling impact on life cycle assessment, Procedia CIRP 29 (2015) 426–431.

[3] D. Paraskevas, K. Kellens, Renaldi, W. Dewulf, J.R. Duflou, Sustainable Metal Management and Recycling Loops: Life Cycle Assessment for Aluminium Recycling Strategies, in: A. Nee, B. Song, S.K. Ong (Eds.), Re-engineering Manufacturing for Sustainability, Springer, Singapore, 2013, pp. 403–408.

[4] L. Donati, B. Reggiani, R. Pelaccia, M. Negozio, S. Di Donato, Advancements in extrusion and drawing: a review of the contributes by the ESAFORM community, Int. J. Mater. Forming 15 (2022) 41.

[5] R. Pelaccia, M. Negozio, S. Di Donato, B. Reggiani, L. Donati, Numerical simulation of the extrusion process with different FEM code approaches: analysis of thermal field, profile speed, defects evolution, and microstructure of hollow tubes, in: Proceedings of ESAFORM Conference on Material Forming, 2024, pp. 771–780.

[6] S. Di Donato, R. Pelaccia, M. Negozio, N. Lai, M. El Mehtedi, B. Reggiani, L. Donati, Effect of material characterization via torsion tests on the accuracy of FEM simulations in the extrusion process, in: Material Forming – ESAFORM 2025, Mater. Res. Proc. 54 (2025) 780–791.

[7] M. Negozio, A. Segatori, R. Pelaccia, B. Reggiani, S. Di Donato, L. Donati, Modeling of recrystallization behaviour of AA6xxx aluminum alloy during extrusion process, Trans. Nonferrous Met. Soc. China 34 (2024) 3170–3184.

[8] M. Negozio, R. Pelaccia, L. Donati, B. Reggiani, S. Di Donato, Microstructure evolution and FEM prediction on AA6XXX alloys, Key Eng. Mater. 987 (2024) 3–10.

[9] S. Di Donato, R. Pelaccia, M. Negozio, M.E. Mehtedi, B. Reggiani, L. Donati, Hot torsion tests of AA6082 alloy, Key Eng. Mater. 988 (2024) 21–29.

[10] M. Negozio, L. Donati, A.H.A. Lutey, Smart extrusion via data-driven prediction of grain size and peripheral coarse grain defect formation, Sci. Rep. 15 (2025) 9518.

[11] X.H. Fan, M. Li, D.Y. Li, Y.C. Shao, S.R. Zhang, Y.H. Peng, Dynamic recrystallisation and dynamic precipitation in AA6061 aluminium alloy during hot deformation, Mater. Sci. Technol. 30 (2014) 1263–1272.

[12] D. Hu, L. Wang, H.J. Wang, Dynamic recrystallization behavior and processing map of the 6082 aluminum alloy, Materials 13 (2020) 1042.

[13] R.H. Buzolin, F. Krumphals, M.C. Poletti, Topological aspects in the microstructural evolution of AA6082 during hot plastic deformation, Eur. J. Mater. 3 (2023) 2218403.

[14] M.C. Poletti, T. Simonet-Fotso, D. Halici, D. Canelo-Yubero, F. Montheillet, D. Piot, et al., Continuous dynamic recrystallization during hot torsion of an aluminum alloy, J. Phys.: Conf. Ser. 1270 (2019) 012049.

[15] Y.C. Lin, L.T. Li, Y.X. Fu, Y.Q. Jiang, Hot compressive deformation behavior of 7075 Al alloy under elevated temperature, J. Mater. Sci. 47 (2012) 1306–1318.

[16] H.E. Hu, L. Zhen, B.Y. Zhang, L. Yang, J.Z. Chen, Microstructure characterization of 7050 aluminum alloy during dynamic recrystallization and dynamic recovery, Mater. Charact. 59 (2008) 1185–1189.

[17] B. Wu, M.Q. Li, D.W. Ma, The flow behavior and constitutive equations in isothermal compression of 7050 aluminum alloy, Mater. Sci. Eng. A 542 (2012) 79–87.

[18] Q. Yang, X. Liu, Y. Liu, X. Fan, M. Shu, The flow softening behavior and deformation mechanism of AA7050 aluminum alloy, Mater. Trans. 60 (2019) 2041–2047.

[19] Y.C. Lin, L.T. Li, Y.Q. Jiang, A phenomenological constitutive model for describing thermo-viscoplastic behavior of Al-Zn-Mg-Cu alloy under hot working condition, Exp. Mech. 52 (2012) 993–1002.

[20] J. Lv, J.-H. Zheng, V.A. Yardley, Z. Shi, J. Lin, A review of microstructural evolution and modelling of aluminium alloys under hot forming conditions, Metals 10 (2020) 1516.